

pubs.acs.org/ac Article

Detector-Free Photothermal Bar-Chart Microfluidic Chips (PT-Chips) for Visual Quantitative Detection of Biomarkers

Wan Zhou, Guanglei Fu, and Xiujun Li*



Cite This: Anal. Chem. 2021, 93, 7754-7762

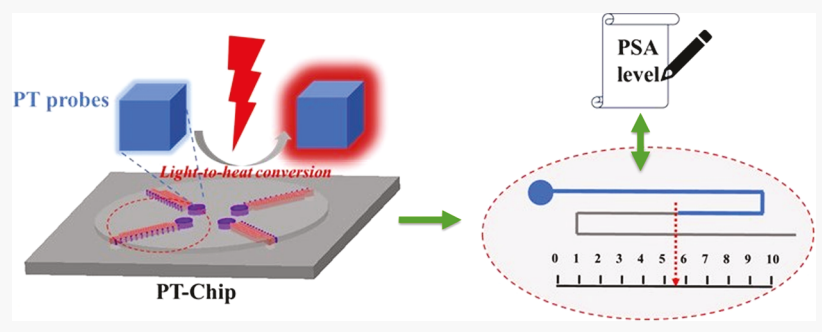


ACCESS

III Metrics & More



Supporting Information



ABSTRACT: The volumetric bar-chart microfluidic chips (V-Chips) driven by chemical reaction-generated gas provide a promising platform for point-of-care (POC) visual biomarker quantitation. However, multiple limitations are encountered in conventional V-Chips, such as costly and complex chip fabrication, complicated chip assembly, and imprecise controllability of gas production. Herein, we introduced nanomaterial-mediated photothermal effects to V-Chips, and for the first time developed a new type of V-Chip, photothermal bar-chart microfluidic chip (PT-Chip), for visual quantitative detection of biochemicals without any bulky and costly analytical instruments. Immunosensing signals were converted to visual readout signals via photothermal effects, the on-chip bar-chart movements, enabling quantitative biomarker detection on a low-cost polymer hybrid PT-Chip with on-chip scale rulers. Four different human serum samples containing a prostate-specific antigen (PSA) as a model analyte were detected simultaneously using the PT-Chip, with a limit of detection of 2.1 ng/mL, meeting clinical diagnostic requirements. Although no conventional signal detectors were used, it achieved comparable detection sensitivity to absorbance measurements with a microplate reader. The PT-Chip was further validated by testing human whole blood without the color interference problem, demonstrating the good analytical performance of our method even in complex matrices and thus the potential to fill the gap in current clinical diagnostics that is incapable of testing whole blood. This new PT-Chip driven by nanomaterial-mediated photothermal effects opens a new horizon of microfluidic platforms for instrument-free diagnostics at the point-of-care.

INTRODUCTION

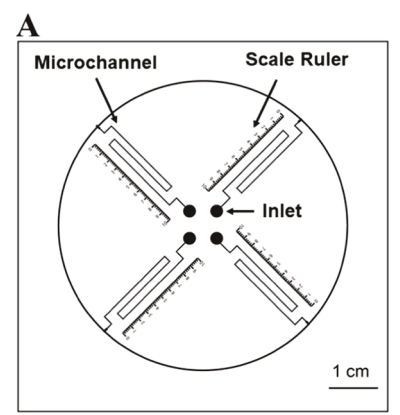
Protein biomarkers play an important role in disease screening, disease diagnosis, prognosis, treatment responses, and therapeutic decisions. 1-3 Currently, various methods have been developed for the detection of protein biomarkers, including surface plasmon resonance (SPR),⁴ colorimetry,^{5,6} fluorescence, electrochemistry, and chemiluminescence. Unfortunately, these conventional methods still face great challenges for point-of-care (POC) applications, especially in resource-limited settings. For instance, colorimetric detection is one of the most widely used methods in enzyme-linked immunosorbent assays (ELISAs), leveraging its simple and visual color changes; whereas the sensitivity and selectivity of colorimetric methods are always compromised. ¹⁰ Additionally, colorimetric methods are vulnerable to color interferences and can only provide qualitative or semiquantitative data, unless a specialized instrument such as a spectrophotometer is used. Such issues also limit the development of near-patient whole

blood testing, which is conducted as closely as possible after specimen collection and eliminates the centrifugation process required in current serological tests. 11,12 Although some other detection methods (e.g., SPR, fluorescence, and electrochemistry) can provide high sensitivity and selectivity, 13 they rely on expensive biochemicals (e.g., enzymes), costly and bulky instruments (e.g., fluorescence microscopy and microplate readers), and trained personnel. Therefore, there has been a sustained need for developing new immunosensing strategies for low-cost, simple, and portable POC detection of protein biomarkers.

Received: March 26, 2021 Accepted: May 4, 2021 Published: May 17, 2021







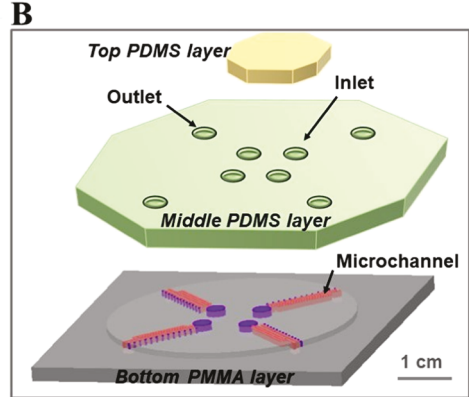


Figure 1. Top view (A) and the exploded view (B) of the PDMS/PMMA hybrid PT-Chip.

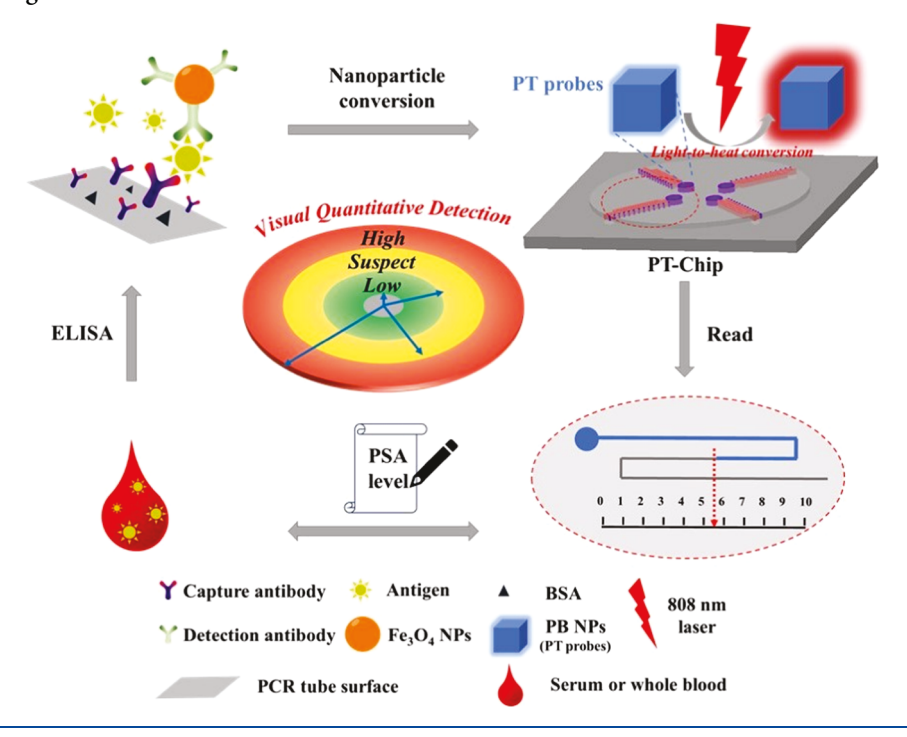
Microfluidic lab-on-a-chip (LOC) technology offers a powerful diagnostic tool for the POC detection of various biomolecules, with various significant advantages such as low reagent consumption, fast assays, miniaturization, high degrees of integration, and portability. 14-21 Recently, a novel POC microfluidic platform has been developed by Qin and coworkers, namely, the volumetric bar-chart microfluidic chip (V-Chip), which shows great potential for visual biochemical quantitation.²² By applying catalase as the ELISA probe, oxygen gas was generated and accumulated within microfluidic channels, leading to increased pressure to push the preloaded ink to move through microfluidic channels in the V-Chip. Because the as-produced moving distances were correlated with the concentrations of protein biomarkers, the V-Chip achieved quantitative measurements of analytes without using costly detectors. By combining different immunoassays with V-Chips, various detection platforms have been explored thereafter to detect a broad range of biomolecular targets, leveraging the convenient analytical readouts.^{22–28} Despite the promising potential of V-Chips in POC testing, there are multiple drawbacks hurdling their wide applications for POC detection and other applications. For example, the fabrication of glass microfluidic V-Chips is complicated, and requires stringent cleanroom facilities, resulting in high cost. Besides, to obtain good sealing of V-Chips, V-Chips are needed to be assembled and aligned in a specific configuration on site by trained personnel, making it challenging for biosensing at the point-of-care. More significantly, all current V-Chips are driven by gas generation via chemical/enzymatic reactions, which lack controllability of reactions once they start and stability due to inevitable denaturation of enzymes at the point-of-care. There is high demand for the development of new types of V-Chips by introducing new types of robust driving forces.

Nanomaterial-mediated photothermal effects have attracted a lot of attention due to the unique light-to-heat conversion property, invasiveness, and compatibility in many biological systems. Photothermal effects have been extensively studied in photothermal cancer therapy for more than two decades, but they have not been explored for biosensing until recently. For example, our group developed the first photothermal immunoassay for the detection of cancer biomarkers using a thermometer, avoiding the need for expensive analytical instruments. Most recently, by applying gold nanoparticle aggregates as photothermal probes, another quantitative biosensing platform was developed for genetic analysis based on the gold nanoparticle aggregation-induced

photothermal effects.⁴⁰ Only using a thermometer, target nucleic acids were quantified with high sensitivity and specificity, where the concentration of target nucleic acids was correlated with the temperature increase upon irradiation of a near-infrared (NIR) laser.⁴⁰ These studies have motivated us to initiate new types of applications of photothermal effects as new driving forces in bar-chart microfluidic chips.

In this work, we applied nanomaterial-mediated photothermal effects to microfluidic chips and developed a new type of V-Chips, photothermal bar-chart microfluidic chip (PT-Chip) driven by photothermal effects, for quantitative biochemical analysis without using any bulky and costly detectors. This photothermal platform was composed of inexpensive materials, poly(methyl methacrylate) (PMMA) and poly(dimethylsiloxane) (PDMS), for the fabrication of hybrid photothermal microfluidic chips. By introducing the iron oxide nanoparticle (Fe₃O₄ NP)-mediated photothermal effect into the volumetric bar-chart microchip, the produced PT-Chip was used for visual quantitative immunosensing of protein biomarkers, without the aid of any detectors. Fe₃O₄ NPs involved in a typical sandwich immunoassay were converted to Prussian blue nanoparticles (PB NPs), a strong NIR photothermal agent. PB NPs were then exploited to generate heat under the laser irradiation, acting as a powerful driving force in the PT-Chip. As such, the immunosensing signals were converted to visual bar charts on the PT-Chip. The quantitation of biomolecules was achieved by visually reading the colored bar-chart distance on the PT-Chip, without the aid of any bulky and expensive instruments. As a model target, a cancer biomarker, prostate-specific antigen (PSA), was spiked in different media (phosphate-buffered saline (PBS) buffer and normal human serum samples) and successfully detected using this PT-Chip. Visual quantitative measurements of PSA were achieved, with the limits of detection (LODs) of 2.0 and 2.1 ng/mL in the PBS buffer and serum samples, respectively. The sensitivity of the on-chip detection of PSA meets the clinical requirement of prostate cancer diagnostics. This method was further validated by testing spiked PSA in human whole blood samples without the issues of color interferences, with satisfactory analytical recoveries. This PT-Chip provides a new low-cost platform for quantitative POC analysis without using costly instruments, with ease of operations, minimal color interferences, and a new robust and controllable driving force.

Scheme 1. Working Principle of the Nanomaterial-Mediated Photothermal Bar-Chart Microfluidic Chip for Visual Quantitative Biosensing



EXPERIMENTAL SECTION

Materials. Chemicals and materials, including bovine serum albumin (BSA), human serum, Dulbecco's phosphate-buffered saline (PBS buffer, 10 mM, pH 7.4), and prostate-specific antigen (PSA), were purchased from Sigma (St. Louis, MO). Other chemicals are listed in SI.

PT-Chip. The PDMS/PMMA hybrid PT-Chip (7.5 cm × 7.5 cm) consisted of three layers, including a top PDMS lid, a middle PDMS layer, and a bottom PMMA layer, as illustrated in the exploded view in Figure 1. Both PDMS layers were fabricated according to a modified soft lithography procedure that we published previously.⁴⁶

The patterned PMMA layer was designed with Adobe AI software, as shown in Figure 1A, including four individual units for photothermal measurements only upon one-time laser irradiation. Each unit contained one microwell acting as both the sample inlet and the laser irradiation spot, one microchannel for sample flowing upon the laser irradiation, and one scale ruler for convenient signal reading. This layer was fabricated from a PMMA sheet (1.5 mm in thickness) using a laser cutter (Epilog laser, Golden, CO). The on-chip scale rulers were customized with each unit equivalent to 2.0 mm. When each layer was ready, the two PDMS layers and the PMMA layer were assembled reversibly based on the selfadhesion (Figure 1B).⁴⁷ Basically, the bottom PMMA layer was sealed first by aligning with the middle PDMS layer. Then, the immunosensing solution was introduced to the PT-Chip through the center inlets. Finally, the top PDMS layer was used to seal the inlets prior to the laser irradiation. More fabrication details are described in SI.

Visual Quantitative Detection of PSA on the PDMS/PMMA Hybrid PT-Chip. The visual quantitative detection of PSA based on the nanoparticle-mediated photothermal effect was performed under the irradiation of an 808 nm diode laser

with a small footprint (Opto Engine, Midvale, UT. $5 \times 2.7 \times$ 1.7"). Four microliters of a food dye solution were added into the above immunosensing solution for enhanced visualization of fluid movements. Each inlet reservoir on the PT-Chip was loaded with 30 μ L of the sample solution and then sealed with the top PDMS layer. Four individual reservoirs containing sample solutions were exposed to the NIR laser at a power density of 2.21 W/cm² simultaneously. The increased vapor pressure originated from the photothermal reagent (PB NPs) would force fluids to flow through the microchannels. Upon laser irradiation for 5 min, the moving distances of colored fluids were observed and recorded directly as bar charts on the PT-Chip. Visual quantitative detection of target PSA was achieved by reading the on-chip moving distance (ΔL) from its corresponding on-chip scale ruler, which was derived from the new driving force provided by nanomaterial-mediated photothermal effects. More assay procedures are described in SI.

RESULTS AND DISCUSSION

Working Principle of the PT-Chip. The nanomaterialmediated photothermal effect was introduced to the PDMS/ PMMA hybrid PT-Chip for the visual quantitative detection of biomarkers. The working principle of the PT-Chip is illustrated in Scheme 1, in which a typical sandwich-type ELISA is applied as a proof of concept, where the monoclonal antibody is immobilized on the PCR tube surface acting as the capture antibody. The prostate cancer biomarker PSA is used as the model target antigen, specifically binding with the capture antibody as well as the Fe₃O₄ NP-labeled polyclonal antibody via immune recognition interactions. In the presence of the target PSA, Fe₃O₄ NPs are introduced and immobilized via the sandwich structure immunoassay. The photothermal effect of Fe₃O₄ NPs was found to be too weak to generate strong photothermal biosensing signals, 48 and thus Fe₃O₄ NPs are converted into a strong NIR photothermal probe (PT probe),

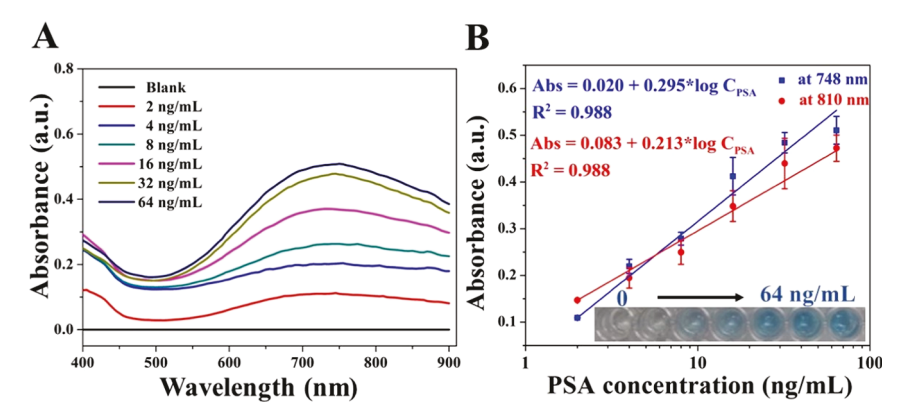


Figure 2. UV-vis characterization of PSA immunoassays in the PBS buffer. (A) UV-vis spectra of immunosensing solutions after the transformation from Fe_3O_4 NPs to PB NPs at different PSA concentrations (0–64 ng/mL) prepared in the PBS buffer. (B) Calibration plots of absorbance at 748 and 810 nm vs the logarithm of the PSA concentration. Insets are the images of the above immunosensing solutions. Error bars represent standard deviations (n = 3).

PB NPs, due to the strong absorption in the NIR region via a simple complexation reaction under acidic conditions (Figure S1). Since the amount of captured Fe₃O₄ NPs is related to the amount of the target, the converted PB NPs are thus correlated with the concentration of the target. After the conversion and the addition of a food dye to enhance the visual effect of the flow movement, the as-prepared solution is loaded into a microwell and sealed in the PT-Chip. When the microwell is irradiated with a NIR laser, the conversion from NIR light to heat is triggered via the nanomaterial-mediated photothermal effect. The heat is accumulated continuously and causes a dramatic increase in vapor pressure in the microwell of the PT-Chip, in which the pressure is transduced to drive colored sample solutions to move into the connected microchannel. It is worth noting that an on-chip scale ruler (with each unit equivalent to 2.0 mm) is designed for the convenience of observation and recording of the moving distance. Because the generated heat is related to the amount of PB NPs, the moving distance of the colored solution is correlated with the original target concentration, thus enabling visual quantitative detection of PSA using the bar-chart distances as detection signals via reading the on-chip scale ruler on the PT-Chip, without using other costly signal detectors. As such, the immunosensing signals are converted to visual quantitative readouts (i.e., on-chip moving distances) using the PT-Chip. In the absence of the target analyte, no specific binding between PSA and capture antibodies occurs. Hence, no Fe₃O₄ NPs are captured or converted to PB NPs, resulting in no noticeable bar-chat movements in microfluidic channels.

Moreover, as shown in Figure 1 and Scheme 1, four separate units are designed in a radial pattern from the center of the PT-Chip. This radial multichannel pattern enables us to perform four individual experiments at the same time with only one-time laser irradiation. Thus, visual quantitative analysis of different targets, different concentrations of one target, or four different replicates of the same sample can be achieved simultaneously from one-time laser irradiation. Although only four channels were designed in this work to demonstrate the proof of the concept, they can be scaled up for higher-throughput visual quantitative analysis without using external detectors.

UV—Vis Characterization of PSA Immunoassays in PBS. To investigate the nanomaterial-mediated immunosensing process, UV—vis spectroscopic characterization was carried

out in a 96-well microplate using a microplate reader. Figure 2 shows the color changes and UV-vis spectra at different concentrations of standard PSA from 0 to 64.0 ng/mL, which were prepared in a PBS buffer (pH 7.4, 10 mM). After the transformation of nanoparticles, it was clearly observed that the color changed from colorless or light yellow to blue (i.e., Prussian blue), when increasing the concentration of PSA in the range from 0 to 64.0 ng/mL. The spectra in Figure 2A exhibited stronger absorbance in the NIR range with the concentration increase of the target, implying the transformation of more Fe₃O₄ NPs into PB NPs and stronger photothermal effects. The peaks at 748 nm proved to be the representative maximum absorbance of PB NPs, which was consistent with the previous literature.⁴⁹ Hence, the color changes and spectra verified the successful transformation from Fe₃O₄ NPs to PB NPs, which was carried in the immunosensing solution in the presence of the analyte. In addition, quantitative colorimetric detection of PSA was performed based on UV-vis absorbance using the microplate reader. Figure 2B displays the calibration curve (blue) between absorbances and concentrations of the target analyte (PSA analyte). The results turned out that the absorbances at 748 nm were proportional to the logarithmical concentrations of PSA spiked in the PBS buffer. A linear relationship was established with the R^2 value of 0.988. The LOD of this colorimetric assay using a microplate reader was calculated to be as low as 1.0 ng/mL based on 3-fold standard deviations above the blank signal, which was comparable to the sensitivity of commercial PSA ELISA kits (LOD: 1.0 ng/mL).⁵⁰ Moreover, the good linearity between absorbances in the NIR range (i.e., at 810 nm) and the logarithmical concentrations of PSA was obtained in Figure 2B (red), which further provided a solid foundation for the following quantitative and sensitive detection of biomarkers based on the photothermal effect-driven principle.

Visual Quantitative Detection of PSA in PBS Using the PDMS/PMMA Hybrid PT-Chip. After the UV—vis absorbance characterization of the PSA immunosensing system, we performed visual quantitative detection of various concentrations of PSA in PBS using the PDMS/PMMA hybrid PT-Chip. Once the immunosensing solutions were loaded to the central microwells on the PDMS/PMMA hybrid PT-Chip, four different samples were irradiated by the 808 nm laser at the same time. With one-time irradiation at the power density

of 2.21 W/cm², all sample solutions started to flow through microchannels due to the photothermal effect-driven principle (Figure 3). The fluid movement could be easily observed by

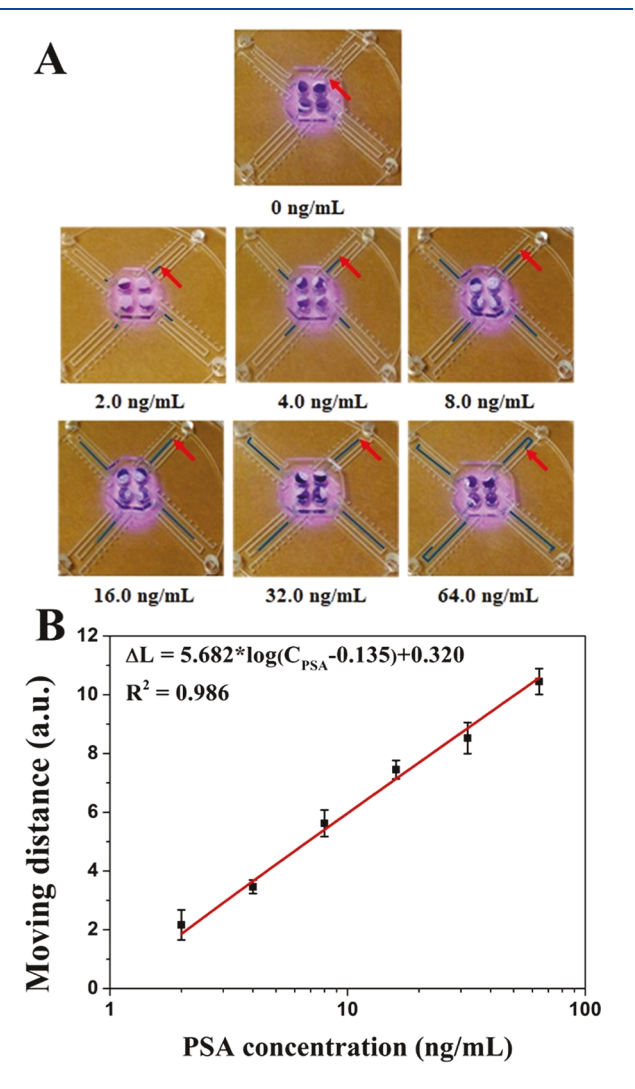


Figure 3. Visual quantitative detection of PSA in PBS using the PDMS/PMMA hybrid PT-Chip. (A) Images of on-chip visual detection of different concentrations of PSA in PBS. Four parallel experiments were conducted simultaneously on a single chip. Red arrows indicate the end location of bar-chart movements. (B) Calibration plot of moving distances (ΔLs) vs the logarithmical concentrations of PSA. Error bars represent standard deviations (n = 4), 1 au = 2.0 mm. The laser irradiation time was 5 min at the laser power density of 2.21 W/cm².

naked eyes, and the moving distance (ΔL) through the microchannels was recorded as the readout according to the designed on-chip scale ruler immediately after the 5 min irradiation. It is noted that the yellow-colored background was used for enhanced visual contrast between the background and the colored bar charts in microfluidic channels. As shown in Figure 3A, with the increase of PSA concentrations, the moving distances of sample solutions were clearly elongated under the laser irradiation. In the control tests (0 ng/mL PSA), the ΔL value was acquired to be minimal (0.54 au), whereas a ΔL value of 10.45 au was observed at the PSA concentration of 64 ng/mL (note: 1 au = 2.0 mm). A linear relationship (Figure 3B) was obtained between the moving distances and the

logarithmical concentrations of PSA in the range from 2.0 to 64.0 ng/mL, with the R^2 value of 0.986. The LOD was determined to be 2.0 ng/mL. Although no bulky and costly instruments were used, our PT-Chip demonstrated similar detection sensitivity to the colorimetric method using a microplate reader (LOD, 1.0 ng/mL), showing great potential for clinical diagnostics with the cutoff PSA concentration of 4.0 ng/mL. This series of studies also built a solid framework for us to move forward to test more complicated human samples.

Colorimetric Immunosensing of PSA in Human Serum Samples Using a Microplate Reader. Human serum is the standard sample used in current clinical diagnostic testing of PSA. 51-53 To validate our method and examine the matrix effects, normal human serum samples spiked with different concentrations of PSA were employed instead of PBS buffers. Similarly, we first tested the feasibility using colorimetric detection of PSA in human serum samples using a microplate reader before the on-chip photothermal bar-chart detection. UV-vis characterization of the colorimetric ELISA of PSA in human serum was performed using a microplate reader, and the results are shown in Figure 4. As the PSA concentration increased, an obvious and enhanced blue color appeared in the sample solutions (Figure 4A), confirming the successful immunorecognition and the subsequent nanoparticle transformation. From the UV-vis spectra (Figure 4B), a calibration curve was obtained between the absorbance at 748 nm and the logarithms of the PSA concentrations (Figure 4C), which were linearly correlated, with an R^2 value of 0.98. The LOD of 1.3 ng/mL PSA was obtained in serum samples, which was similar to the LOD (1.0 ng/mL) obtained in PBS buffers, indicating the feasibility for our subsequent PT-Chip immunosensing of human samples.

Visual Quantitative Detection of PSA in Human Serum Samples Using the PDMS/PMMA Hybrid PT-**Chip.** After demonstrating the feasibility of using UV-vis absorbance, we explored the visual quantitative detection of PSA in human serum samples using the PDMS/PMMA hybrid PT-Chip. In the on-chip detection, under the NIR laser irradiation, the moving distance (ΔL) of varying concentrations of PSA spiked in normal serum samples was recorded. The results in Figure 5A show that the moving distance of sample solutions was prolonged on the PT-Chip as the PSA concentrations increased. The moving distance was proportional to the concentration of PSA in spiked serum samples upon laser irradiation for 5 min. There was a linear relationship between ΔL and the logarithmical concentration of PSA in the range from 1.0 to 64.0 ng/mL, with the coefficient of determination as 0.986 in Figure 5B. The LOD was calculated to be 2.1 ng/mL, which was below the clinical threshold value of 4.0 ng/mL. This LOD is similar to that of the on-chip PSA testing in PBS (2.0 ng/mL) as well as the LOD value from the absorbance measurement of serum samples (1.3 ng/mL). The results confirmed that visual quantitative detection of PSA can be achieved using the PT-Chip, even in complex media such as human serum samples without compromising the detection sensitivity, indicating the robustness of our immunosensing method.

Specificity Tests and Analytical Recoveries. To study the specificity of the photothermal bar-chart chip method, some common interfering substances, including serum, human whole blood, hepatitis B surface antigen (HBsAg), carcinoembryonic antigen (CEA), and immunoglobulin G (IgG) with higher concentrations up to 80 ng/mL, were prepared and

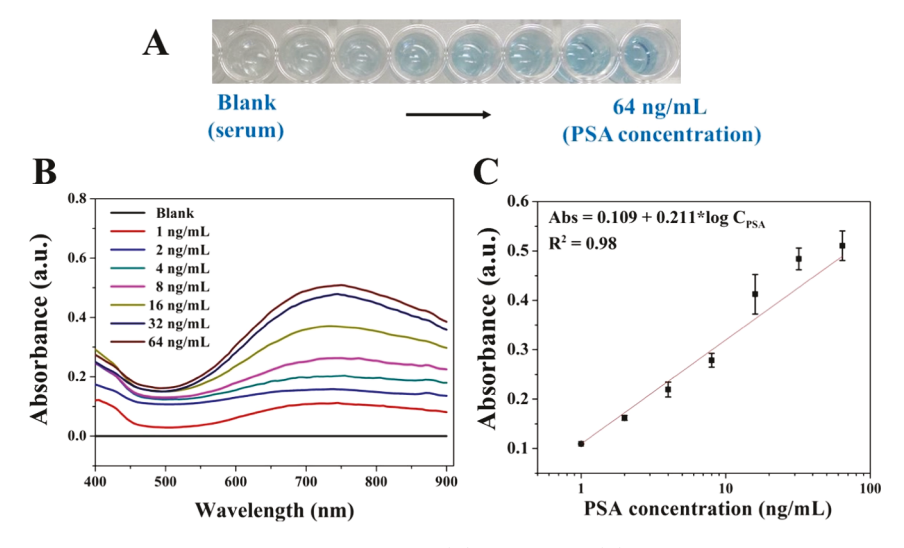


Figure 4. UV-vis characterization of PSA detection in serum samples. (A) Images and (B) UV-vis spectra of immunosensing solutions after the transformation from Fe_3O_4 NPs to PB NPs at different PSA concentrations (0–64 ng/mL) spiked in serum samples. (C) Calibration plot of absorbance at 748 nm vs the logarithm of the PSA concentration. Error bars represent standard deviations (n = 3).

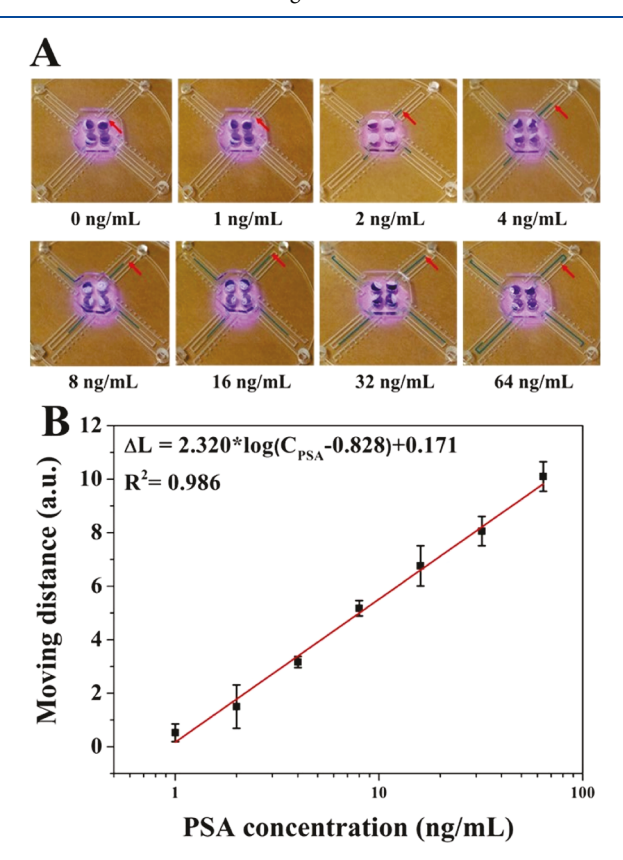


Figure 5. Visual quantitative detection of PSA spiked in human serum samples using the PDMS/PMMA hybrid PT-Chip. (A) Images of onchip detection of different concentrations of PSA spiked in human serum samples. Four parallel experiments were conducted on a single chip at the same time. Red arrows indicate the stop point of bar charts. (B) Calibration plot of moving distances (ΔLs) vs the logarithmical concentrations of spiking PSA. Error bars represent standard deviations (n = 4), 1 au = 2.0 mm. The laser irradiation time was 5 min at the laser power density of 2.21 W/cm².

tested using a similar procedure on the PT-Chip. As shown in Figure 6, compared with blank samples containing only serum or blood matrix media, only samples spiked with PSA had an

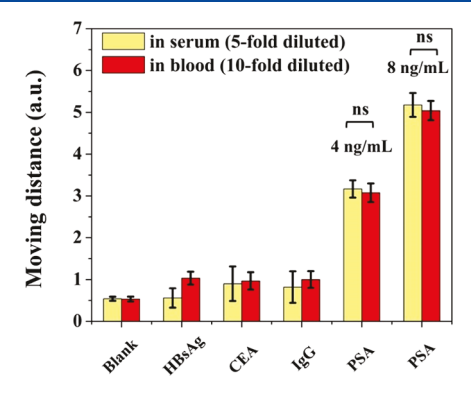


Figure 6. Specificity tests for PSA detection using the PT-Chip in different matrix media, including 5-fold diluted normal human serum and 10-fold diluted human whole blood samples. Other interfering substances were tested including HBsAg, CEA, and IgG with a spiked concentration of 80 ng/mL. The media (serum and whole blood) were used as the blanks. Error bars represent standard deviations (n = 4). The symbol (ns) indicates no statistical significance in the t-test (P-value > 0.05).

obvious moving distance (in the range of 3–6 au), whereas no significant bar-chart movements were observed from other interfering substances, indicating high specificity of our PT-Chip method.

To further evaluate the analytical performance of the photothermal bar-chart chip method in complex media, we also compared the PT-Chip testing results between human serum and human whole blood samples spiked with different concentrations of PSA. Two concentrations of PSA, 4 and 8 ng/mL, were selected in this comparison according to the commonly used threshold concentration and the suspect level for clinical prostate cancer diagnostics. 54-56 As shown in Figure 6, 4.0 ng/mL PSA gave bar-chart values of 3.17 and 3.08 au from serum and whole blood, respectively, while 8.0 ng/mL PSA gave bar-chart values of 5.18 and 5.04 au from serum and whole blood, respectively. Besides, the t-test statistics further confirmed that the results between serum and whole blood were similar, with P values of 0.58 and 0.48 (P-value > 0.05). The results demonstrated high tolerance of our visual quantitative PT-Chip method to matrix effects from

complex media. Furthermore, no color interferences were observed in the whole blood tests using our PT-Chip. Given that current diagnostic methods require the use of serum due to the color interference problem from red blood cells, our visual photothermal bar-chart method is capable of testing whole blood directly, which may fill a gap in the current clinical diagnostics paradigm.

Furthermore, our PT-Chip method was validated by testing the analytical recoveries of PSA spiked in serum and human whole blood samples. Similarly, we chose two PSA concentrations at the cutoff level and the suspect level in both matrix samples (i.e., 4.0 and 8.0 ng/mL, respectively). By comparing the known spiked concentrations in the immunoassay and the measured values of PSA using the PT-Chip, the analytical recoveries were calculated and summarized in Table S1. It was found that the analytical recoveries with PSA concentrations of 4.0 and 8.0 ng/mL in the human serum were 91.3-91.9%, respectively. The analytical recoveries obtained in spiked human whole blood samples were 92.5-89.1%, respectively. Their RSD values ranged from 4.5 to 7.0%. Overall, all of the analytical recoveries were within the acceptable criteria for bioanalytical method validation, 57,58 indicating that our PT-Chip yields reliable results with satisfactory interpretation for the detection of PSA even in the human whole blood matrix.

CONCLUSIONS

In conclusion, photothermal effects as a new type of driving force have been for the first time applied to V-Chip, and thus an innovative photothermal bar-chart microfluidic chip (PT-Chip) has been developed for visual quantitative detection of multiple biochemicals at the point-of-care, without the use of any costly and bulky instruments. PSA as a model analyte was successfully detected using this PT-Chip from different types of matrices, including PBS buffers, human serum, and human whole blood samples, with high sensitivity and specificity. The LOD of 2.1 ng/mL PSA was obtained in normal human serum samples, which met the cutoff requirement in clinical diagnostics for prostate cancers. This detection platform was further validated by testing spiked human whole blood samples, obtaining satisfactory analytical recoveries, demonstrating good analytical performance for biomarker detection even in the complex matrix.

This new type of V-Chip, PT-Chip, has many significant features. (1) It is miniaturized, portable, and does not require any costly and bulky conventional analytical instruments, enhancing the capability for POC detection in various settings, especially for those resource-poor settings, such as households, small clinics, rural areas, and developing nations. The performance comparison between the PT-Chip and other methods for PSA quantitation is summarized in Table S2. It can be seen that although our PT-Chip method does not require any detectors, it provides comparable or even higher sensitivity and a relatively broader dynamic range, compared to most colorimetric immunoassays using microfluidics and commercial colorimetric ELISA kits. (2) The produced signals (i.e., on-chip bar-chart movements) are easy to visualize, read, and record, with no need for trained personnel and complex data analytics. (3) Compared to the conventional gas-driven V-Chips based on chemical reactions, the PT-Chip using nanomaterial-mediated photothermal effects as the driving force has precise controllability in controlling reaction progresses and the location of the reactions on the chip,

which can be remotely tuned by adjusting parameters of laser irradiation. Relevant work with high degrees of integration is underway in our laboratory. (4) Given the nature of the readout based on bar-chart movement instead of color changes, the PT-Chip has unique advantages in quantitative POC detection of colored samples without interference problems. As demonstrated in this work, PSA was successfully detected in human whole blood, without noticeable differences from serum testing results. Because current diagnostic methods require precentrifugation to obtain serum before biomarker assays, our PT-Chip capable of whole blood testing can fill a gap in the conventional clinical diagnostics paradigm. (5) The fabrication of the PT-Chip is simple and low cost due to the use of inexpensive materials (i.e., PDMS and PMMA), as compared with glass-based V-Chips that require a cleanroom and complex and costly fabrication procedures. No specialized infrastructure (like cleanroom) and complicated assembly processes are needed. (6) Multiple microwells from the PT-Chip allow the versatile and multiplexed detection of multiple analytes/samples simultaneously. Although only four analytical units are designed in our current PT-Chip, more analytical units can be scaled up. Overall, by combining nanomaterialmediated photothermal effects with microfluidic LOC devices, the PT-Chip has great potential in the exploration of new POC diagnostic tools for broad applications, particularly given more inexpensive, portable, and powerful laser pointers becoming commercially available recently. The novel introduction of nanomaterial-mediated photothermal effects into bar-chart microfluidic chips opens a new era toward advances in clinical diagnostics and POC analysis, as well as for the exploration of new application fields of photothermal effects.

ASSOCIATED CONTENT

Supporting Information

The Supporting Information is available free of charge at https://pubs.acs.org/doi/10.1021/acs.analchem.1c01323.

Material details, the fabrication of the PDMS/PMA hybrid PT-Chip, the preparation of the antibody-conjugated Fe_3O_4 NPs, nanomaterial-mediated immunosensing procedures, nanoparticle transformation procedures and the schematic illustration, analytical recoveries, and performance comparison (PDF)

AUTHOR INFORMATION

Corresponding Author

Xiujun Li — Department of Chemistry and Biochemistry, The University of Texas at El Paso, El Paso, Texas 79968, United States; Border Biomedical Research Center, Biomedical Engineering and Environmental Science and Engineering, The University of Texas at El Paso, El Paso, Texas 79968, United States; ◎ orcid.org/0000-0002-7954-0717; Email: xli4@ utep.edu

Authors

Wan Zhou − Department of Chemistry and Biochemistry, The University of Texas at El Paso, El Paso, Texas 79968, United States; ocid.org/0000-0002-1439-9548

Guanglei Fu — Department of Chemistry and Biochemistry, The University of Texas at El Paso, El Paso, Texas 79968, United States; Biomedical Engineering Research Center, Medical School of Ningbo University, Ningbo, Zhejiang 315211, P. R. China; orcid.org/0000-0002-8128-1224

Complete contact information is available at: https://pubs.acs.org/10.1021/acs.analchem.1c01323

Author Contributions

¹W.Z. and G.F. contributed equally.

Notes

The authors have a patent pending.

The authors declare the following competing financial interest(s): A patent has been filed.

ACKNOWLEDGMENTS

The authors would like to acknowledge the financial support from the National Institute of Allergy and Infectious Disease of the NIH (R21AI107415), the U.S. NSF (IIP2052347 and IIP1953841), DOT (CARTEEH), the University of Texas at El Paso (UTEP) for the IDR Program, the Philadelphia Foundation, and the Medical Center of the Americas Foundation. They are also grateful for the financial support to their prior research from the National Institute of General Medical Sciences of the NIH (SC2GM105584), the NIH RCMI Pilot grant, the NIH BUILDing Scholar Summer Sabbatical Award, NSF (DMR1827745), the University of Texas (UT) System for the STARS Award, and UTEP for the Multidisciplinary Research Award Program (MRAP) and the URI Program.

REFERENCES

- (1) Strimbu, K.; Tavel, J. A. Curr. Opin. HIV AIDS 2010, 5, 463-466.
- (2) Ganna, A.; Salihovic, S.; Sundstrom, J.; Broeckling, C. D.; Hedman, A. K.; Magnusson, P. K. E.; Pedersen, N. L.; Larsson, A.; Siegbahn, A.; Zilmer, M.; Prenni, J.; Arnlov, J.; Lind, L.; Fall, T.; Ingelsson, E. *PLoS Genet.* **2014**, *10*, No. e1004801.
- (3) Topkaya, S. N.; Azimzadeh, M.; Ozsoz, M. Electroanalysis 2016, 28, 1402-1419.
- (4) Zou, F. M.; Zhou, H. J.; Tan, T. V.; Kim, J.; Koh, K.; Lee, J. ACS Appl. Mater. Interfaces 2015, 7, 12168–12175.
- (\$) Qu, F. L.; Li, T.; Yang, M. H. Biosens. Bioelectron. 2011, 26, 3927-3931.
- (6) Fu, G.; Sanjay, S. T.; Zhou, W.; Brekken, R. A.; Kirken, R. A.; Li, X. Anal. Chem. **2018**, *90*, 5930–5937.
- (7) Chinen, A. B.; Guan, C. M.; Ferrer, J. R.; Barnaby, S. N.; Merkel, T. J.; Mirkin, C. A. Chem. Rev. 2015, 115, 10530-10574.
- (8) Chikkaveeraiah, B. V.; Bhirde, A. A.; Morgan, N. Y.; Eden, H. S.; Chen, X. ACS Nano 2012, 6, 6546–6561.
- (9) Bi, S.; Zhou, H.; Zhang, S. S. Biosens. Bioelectron. 2009, 24, 2961–2966.
- (10) Sanjay, S. T.; Fu, G. L.; Dou, M. W.; Xu, F.; Liu, R. T.; Qi, H.; Li, X. J. Analyst 2015, 140, 7062-7081.
- (11) Ritchie, A. V.; Goel, N.; Sembongi, H.; Lehga, J.; Farleigh, L. E.; Edemaga, D.; Wisniewski, C. A.; Lee, H. H. *J. Virol. Methods* **2016**, 237, 143–149.
- (12) Schultz, N. A.; Dehlendorff, C.; Jensen, B. V.; Bjerregaard, J. K.; Nielsen, K. R.; Bojesen, S. E.; Calatayud, D.; Nielsen, S. E.; Yilmaz, M.; Hollander, N. H.; Andersen, K. K.; Johansen, J. S. *Jama* **2014**, 311, 392–404.
- (13) Lv, M.; Zhou, W.; Tavakoli, H.; Bautista, C.; Xia, J.; Wang, Z.; Li, X. Biosens. Bioelectron. 2021, 176, No. 112947.
- (14) Dou, M. W.; Sanjay, S. T.; Benhabib, M.; Xu, F.; Li, X. J. *Talanta* **2015**, *145*, 43–54.
- (15) Zhou, W.; Feng, M.; Valadez, A.; Li, X. Anal. Chem. 2020, 92, 7045–7053.
- (16) Prasad, K. S.; Cao, X.; Gao, N.; Jin, Q.; Sanjay, S. T.; Henao-Pabon, G.; Li, X. Sens. Actuators, B 2020, 305, No. 127516.
- (17) Tavakoli, H.; Zhou, W.; Ma, L.; Perez, S.; Ibarra, A.; Xu, F.; Zhan, S.; Li, X. TrAC, Trends Anal. Chem. 2019, 13-26.

- (18) Tavakoli, H.; Zhou, W.; Ma, L.; Guo, Q.; Li, X. Nanotechnol. Microfluid. 2020, 177-209.
- (19) Wei, X.; Zhou, W.; Sanjay, S. T.; Zhang, J.; Jin, Q.; Xu, F.; Dominguez, D. C.; Li, X. Anal. Chem. **2018**, 90, 9888–9896.
- (20) Sanjay, S. T.; Zhou, W.; Dou, M. W.; Tavakoli, H.; Ma, L.; Xu, F.; Li, X. J. Adv. Drug Delivery Rev. 2018, 128, 3–28.
- (21) Li, Z.; You, M.; Bai, Y.; Gong, Y.; Xu, F. Small Methods 2020, 4, No. 1900459.
- (22) Song, Y.; Zhang, Y.; Bernard, P. E.; Reuben, J. M.; Ueno, N. T.; Arlinghaus, R. B.; Zu, Y.; Qin, L. Nat. Commun. 2012, 3, No. 1283.
- (23) Song, Y. J.; Xia, X. F.; Wu, X. F.; Wang, P.; Qin, L. D. Angew. Chem., Int. Ed. 2014, 53, 12451–12455.
- (24) Song, Y.; Li, Y.; Qin, L. Methods Mol. Biol. 2017, 1570, 105-115.
- (25) Zhu, Z.; Guan, Z. C.; Jia, S. S.; Lei, Z. C.; Lin, S. C.; Zhang, H. M.; Ma, Y. L.; Tian, Z. Q.; Yang, C. J. Angew. Chem., Int. Ed. 2014, 53, 12503–12507.
- (26) Wang, Y. Z.; Zhu, G. X.; Qi, W. J.; Li, Y.; Song, Y. J. Biosens. Bioelectron. 2016, 85, 777-784.
- (27) Song, Y. J.; Wang, Y. Z.; Qi, W. J.; Li, Y.; Xuan, J.; Wang, P.; Qin, L. D. Lab Chip 2016, 16, 2955–2962.
- (28) Li, Y.; Xuan, J.; Xia, T.; Han, X.; Song, Y. J.; Cao, Z.; Jiang, X.; Guo, Y.; Wang, P.; Qin, L. D. Anal. Chem. 2015, 87, 3771–3777.
- (29) Fu, G.; Zhu, Y.; Wang, W.; Zhou, M.; Li, X. ACS Sens. 2019, 4, 2481–2490.
- (30) Fu, G. L.; Zhu, Y. B.; Xu, K.; Wang, W. H.; Hou, R. X.; Li, X. J. Anal. Chem. **2019**, 91, 13290–13296.
- (31) Fu, G. L.; Sanjay, S. T.; Zhou, W.; Brekken, R. A.; Kirken, R. A.; Li, X. J. Anal. Chem. **2018**, *90*, 5930–5937.
- (32) Hong, G. L.; Zhang, D. D.; He, Y. H.; Yang, Y. Y.; Chen, P.; Yang, H. J.; Zhou, Z. Y.; Liu, Y. H.; Wang, Y. Anal. Bioanal. Chem. **2019**, 411, 6837–6845.
- (33) Du, S. Y.; Wang, Y.; Liu, Z. C.; Xu, Z. X.; Zhang, H. Y. Biosens. Bioelectron. 2019, 144, No. 111670.
- (34) Fu, G. L.; Sanjay, S. T.; Li, X. J. Analyst 2016, 141, 3883-3889.
- (35) You, M.; Li, Z.; Feng, S.; Gao, B.; Yao, C.; Hu, J.; Xu, F. Trends Biotechnol. **2020**, 38, 637–649.
- (36) You, M.; Cao, L.; Xu, F. Trends Biochem. Sci. 2020, 45, 174-175.
- (37) You, M.; Jia, P.; He, X.; Wang, Z.; Feng, S.; Ren, Y.; Li, Z.; Cao, L.; Gao, B.; Yao, C.; et al. *Small Methods* **2021**, No. 2001254.
- (38) Fu, G.; Sanjay, S. T.; Dou, M.; Li, X. Nanoscale **2016**, 8, 5422–5427.
 - (39) Zhang, J.; Xing, H.; Lu, Y. Chem. Sci. 2018, 9, 3906-3910.
- (40) Zhou, W.; Hu, K. Q.; Kwee, S.; Tang, L.; Wang, Z. H.; Xia, J. F.; Li, X. J. Anal. Chem. **2020**, 92, 2739–2747.
- (41) Zhou, W.; Sun, J.; Li, X. Anal. Chem. 2020, 92, 14830-14837.
- (42) Fu, G.; Zhou, W.; Li, X. Lab Chip 2020, 20, 2218-2227.
- (43) Hastman, D. A.; Melinger, J. S.; Aragones, G. L.; Cunningham, P. D.; Chiriboga, M.; Salvato, Z. J.; Salvato, T. M.; Brown, C. W., 3rd; Mathur, D.; Medintz, I. L.; Oh, E.; Diaz, S. A. ACS Nano 2020, 14, 8570–8583.
- (44) Liu, Y.; Pan, M.; Wang, W.; Jiang, Q.; Wang, F.; Pang, D. W.; Liu, X. Anal. Chem. 2019, 91, 2086–2092.
- (45) Huang, L.; Chen, J.; Yu, Z.; Tang, D. Anal. Chem. 2020, 92, 2809–2814.
- (46) Dou, M. W.; Sanjay, S. T.; Dominguez, D. C.; Liu, P.; Xu, F.; Li, X. J. Biosens. Bioelectron. **2017**, 87, 865–873.
- (47) Gajasinghe, R. W. R. L.; Senveli, S. U.; Rawal, S.; Williams, A.; Zheng, A.; Datar, R. H.; Cote, R. J.; Tigli, O. *J. Micromech. Microeng.* **2014**, *24*, No. 075010.
- (48) Fu, G.; Liu, W.; Feng, S.; Yue, X. Chem. Commun. 2012, 48, 11567–11569.
- (49) Fu, G.; Sanjay, S. T.; Li, X. Analyst 2016, 141, 3883-3889.
- (50) Gao, Z.; Hou, L.; Xu, M.; Tang, D. Sci. Rep. 2015, 4, No. 3966.
- (51) Chen, H.; Li, Z.; Zhang, L.; Sawaya, P.; Shi, J.; Wang, P. Angew. Chem. 2019, 131, 14060–14066.
- (52) Sathianathen, N. J.; Konety, B. R.; Crook, J.; Saad, F.; Lawrentschuk, N. Nat. Rev. Urol. 2018, 15, 627–642.

- (53) Yang, L.; Zheng, J.; Zou, Z.; Cai, H.; Qi, P.; Qing, Z.; Yan, Q.; Qiu, L.; Tan, W.; Yang, R. Chem. Commun. 2020, 56, 1843–1846.
- (54) Bartsch, G. Urology 2002, 59, 893-894.
- (55) Anastasiadis, A. G.; Lichy, M. P.; Nagele, U.; Kuczyk, M. A.; Merseburger, A. S.; Hennenlotter, J.; Corvin, S.; Sievert, K. D.; Claussen, C. D.; Stenzl, A.; Schlemmer, H. P. Eur. Urol. 2006, 50, 738–749
- (56) Aigner, F.; Pallwein, L.; Junker, D.; Schäfer, G.; Mikuz, G.; Pedross, F.; Mitterberger, M. J.; Jaschke, W.; Halpern, E. J.; Frauscher, F. J. Urol. 2010, 184, 913–917.
- (57) Zhou, S.; Zheng, W.; Chen, Z.; Tu, D.; Liu, Y.; Ma, E.; Li, R.; Zhu, H.; Huang, M.; Chen, X. Angew. Chem., Int. Ed. 2014, 53, 12498–502.
- (58) Tiwari, G.; Tiwari, R. Pharm. Methods 2010, 1, 25-38.